Case Studies in Construction Materials 18 (2023) e02003

Contents lists available at ScienceDirect

Case Studies in Construction Materials

journal homepage: www.elsevier.com/locate/cscm

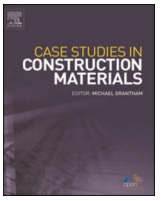

Case study

Reliability-based structural assessment of historical masonry arch bridges: The case study of Cernadela bridge

O. Bouzas [a,*], B. Conde [a], J.C. Matos [b], M. Solla [a], M. Cabaleiro [a]

[a] CINTECX, Universidade de Vigo, GeoTECH Group, Campus Universitario de Vigo, As Lagoas, Marcosende, 36310 Vigo, Spain
[b] Department of Civil Engineering, ISISE, University of Minho, Guimarães, Portugal

ARTICLE INFO

Keywords:
Masonry arch bridges
Geomatic techniques
Limit analysis
Reliability analysis

ABSTRACT

Nowadays, several historical masonry arch bridges present a deficient state of conservation due to degradation processes induced by natural or human actions. Usually, these constructions have significant economic, cultural, and heritage value. Therefore, they shall be thoroughly assessed to verify their structural integrity and safety condition. For this purpose, reliability-based structural assessments are typically performed. However, the associated outcomes (i.e., reliability index and probability of failure) highly rely on the accuracy of the structural parameters uncertainty quantification. This work presents a study regarding the influence of the scattering of the arches' thickness dimensions in the load-carrying capacity assessment of the Cernadela Bridge, a historical stone bridge located in Galicia, Spain. The study first involved a comprehensive experimental campaign to characterize the outer and inner bridge geometry through geomatic techniques, i.e., terrestrial laser scanning and ground penetrating radar. Subsequently, a limit analysis model was developed, considering only the arches' outer (visible) data. From this initial structural assessment, a reliability index of 2.38 was obtained. The influence of the uncertain structural parameters, both geometric features and material properties, in the collapse load was investigated through a global variance-based sensitivity analysis (i.e., Sobol' indices) complemented by a surrogate modeling strategy based on the Kriging approach. Finally, the measured inner geometry of the arches was introduced in the computational model through Bayesian inference procedures. Thus, two new structural assessments were performed: first, by considering the updated distributions of all arches thicknesses, and second, by considering only the updated distributions of the non-influential ones. Reliability indexes of 1.51 and 2.33 were derived, thus highlighting the importance of a proper uncertainty quantification process and the relevance of the sensitivity analysis outcomes to identify the critical parameters on the bridge mechanical response.

1. Introduction

Many masonry arch bridges have stood for centuries since they were built to play an essential role within road and rail networks. In Galicia, in the northwest of Spain, hundreds of bridges dating from the Mediaeval and the Roman ages are still in use because of the irregular topography and the dispersion of settlements. However, due to the degradation processes caused by aging, their conservation state is usually deficient. Besides, due to modern transport, these bridges are subjected to much higher loads and intensive vibrations

* Corresponding author.
E-mail address: oscar.bouzas.rodriguez@uvigo.es (O. Bouzas).

https://doi.org/10.1016/j.cscm.2023.e02003
Received 28 December 2022; Received in revised form 5 March 2023; Accepted 15 March 2023
Available online 16 March 2023

than those for which they were initially designed. Therefore, reliable structural assessment methodologies should be developed and applied to properly assess their actual safety level.

In this regard, different methods have been proposed so far to conduct the masonry arch bridges (MAB) structural assessment. In [1], Sarhosis et al. conducted an in-depth review of several techniques (i.e., semi-empirical, equilibrium-based, and numerical methods) and described their advantages and disadvantages. As for the semi-empirical methods, the MEXE technique, based on the classic elastic arch theory combined with the results of a series of experimental tests [2], has been widely employed. However, as Sarhosis et al. point out, underestimating the load-carrying capacity is one of its main drawbacks. On the other hand, numerical methods based on finite elements (FE) or discrete elements (DE) have shown excellent performance but require huge amounts of computational resources and time. The contributions [3,4] and [5,6] are remarkable examples of applying these techniques for MAB assessments. To achieve an equilibrium between computational efficiency and results accuracy, simplified methods such as the limit analysis method, which discretizes the masonry structure in ideal blocks, can be adopted. Due to its equilibrium-based nature, the collapse load and the reaction forces can be estimated by solving the static equilibrium equations. Its suitability for MAB structural assessment has been demonstrated in numerous previous research works [7–9]. Nonetheless, it should be noted that masonry is a quasi-brittle material, so size-scale effects can play an important role in fracture toughness and propagation. In a limit analysis model, masonry has no tensile strength. Thus, to consider these effects, an evolutionary fracture analysis approach, which relies on Linear Elastic Fracture Mechanics (LEFM), should be used instead [10,11].

On the other hand, the structural evaluation process can be carried out through deterministic or probabilistic approaches. Nowadays, deterministic or semi-probabilistic structural assessment approaches based on partial safety factors are widely used. Nevertheless, due to the degradation processes, aging masonry structures show considerable uncertainties in their parameters, which significantly influence the in-plane [12] and out-of-plane [13] behavior and capacity. These methodologies cannot adequately tackle these uncertainties, which might lead to inaccurate predictions and wrong estimations of the actual load-bearing capacity. Hence, reliability-based structural evaluation approaches, which explicitly consider the uncertainty sources, should be used to increase the assessment confidence and robustness. Several authors have adopted this approach in the civil engineering domain to evaluate aging bridges [14–16]. However, the trustworthiness of reliability-based structural evaluation results strongly relies on the accuracy of the parameters uncertainties' definitions. Typically, these uncertainties can be defined based on information extracted from the literature or experimentally through laboratory testing on specimens extracted from the structure. Nevertheless, in heritage constructions, there is a non-intrusion requirement. To address this challenge, several authors have proved the suitability of experimental characterization of structural parameters using non-destructive testing techniques (NDTs) [17,18]. Within the masonry arch bridges context, the dimensions of the arches voussoirs greatly impact the structural behavior, with a direct relationship between this parameter and the ultimate load-carrying capacity of the construction. The voussoirs are structural elements that usually present significant scattering. Thus, the voussoirs placed near the spandrel walls typically present larger dimensions than those located below the infill, so defining their actual dimensions is very cumbersome. However, modeling them only according to their external geometry would lead to an overestimation of the voussoirs' dimensions and, consequently, of the ultimate load-carrying capacity of the bridge.

This paper analyzes the impact of different levels of knowledge on the geometrical parameters, namely regarding the arches thicknesses, on the load-carrying capacity assessment of masonry bridges using a probabilistic-based structural analysis procedure. The methodology is applied to the Cernadela Bridge, a historical stone bridge in Galicia, Spain. Two different NDTs are used to characterize the external and internal geometry of the arches voussoirs. On the one hand, the external geometry is measured through terrestrial laser scanning (TLS) [19–21]. On the other hand, ground penetrating radar (GPR) technology is used to capture the inner geometry [22–24]. For the initial reliability-based assessment, the uncertainty quantification is described by attending only to the external geometry gathered through the TLS, where a limit analysis model is developed considering only these outer (visible) data. The influence of the uncertain structural parameters, both geometric features and material properties, in the collapse load is also investigated through a comprehensive global variance-based sensitivity analysis (i.e., Sobol' indices) complemented by a surrogate modeling strategy based on the Kriging approach. Considering the identified critical parameters and the internal experimental (geometrical) data from the GPR, the uncertainty definition is finally updated using Bayesian inference procedures. Thus, the statistical definition of the arches thicknesses parameters is improved, achieving more reliable uncertainty definitions. Additional structural assessments are performed, considering the updated random variables so that the different reliability indexes can be compared and proper conclusions can be drawn.

2. Case study

2.1. Historical background and bridge description

The Cernadela Bridge (Fig. 1), located in Galicia, northwest of Spain, is a stone arch bridge that crosses the Tea river to connect the municipalities of Mondariz and Riofrío. According to [25], some historians claim that the bridge was built during the Roman Ages due to the discovery of a roman path in the area. Nevertheless, considering its typology, it is argued that it was probably constructed between the centuries XIV-XV [25]. During the centuries XVII-XVIII, the cutwaters of the bridge were restored, and in the century XX, a section of the bridge collapsed, according to some historical information. Nowadays, the Cernadela Bridge is integrated into the Natura 2000, a network that protects natural habitats. Besides, it was declared an asset of cultural interest in Galicia, proclaiming its heritage and landscaping value [26].

The construction presents five arches, four pointed arches, and a semicircle (see Fig. 2). Regarding the pavement, it has a double-slope shape, and it is made of irregular granite slabs. The bridge has two abutments and four piers. Two pillars have upstream and

Fig. 1. Overall view of Cernadela Bridge.

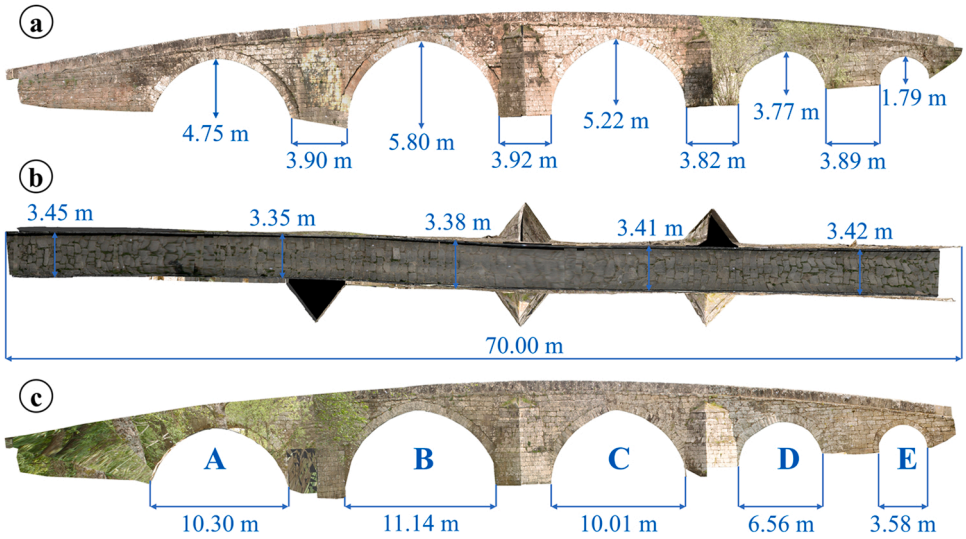

Fig. 2. Orthoimages of Cernadela Bridge: (a) Downstream view, with the rise of arches and width of piers (b) Top view, depicting the total length and bridge width (c) Upstream view, showing arches nomenclature and length of spans.

downstream cutwaters with triangular sections and small pyramidal hats. Besides, the left pier from the upstream view has an additional cutwater that may have been built posteriorly. The infill of the structure is enclosed by regular course masonry spandrels, on which two 0.80 m high and 0.25 m wide parapets are placed over. The whole structure has a total length of almost 70.00 m and a width of approximately 3.40 m (see Fig. 2).

2.2. *Visual inspection*

Previous research [25] concluded that the conservation state of the Cernadela Bridge was deficient. Therefore, a visual inspection was conducted to evaluate the bridge's current condition. Accordingly, a damage mapping was elaborated, recording every defect, its position, and its potential influence on the mechanical response.

The bridge presents an important accumulation of vegetation in the cutwaters, spandrel walls, and arches. This accumulation could be especially harmful in the joints between stones, as it may lead to cracking appearance and separation of structural elements. Additionally, some humidity concentrations were identified in the arches, which might accelerate the degradation process of the voussoirs. Concerning the structural elements, as Lubowiecka et al. [20] mentioned, some arches present cracks and partial detachments. Besides, out-of-plane deformations in the spandrel walls and a noticeable variation in the intrados curvature of arch D were observed. In this regard, the downstream spandrel between arches A and B presents significant transverse deformations, which may be caused by the lateral pressure exerted by the infill. A brief detailing of all these issues can be observed in Fig. 3.

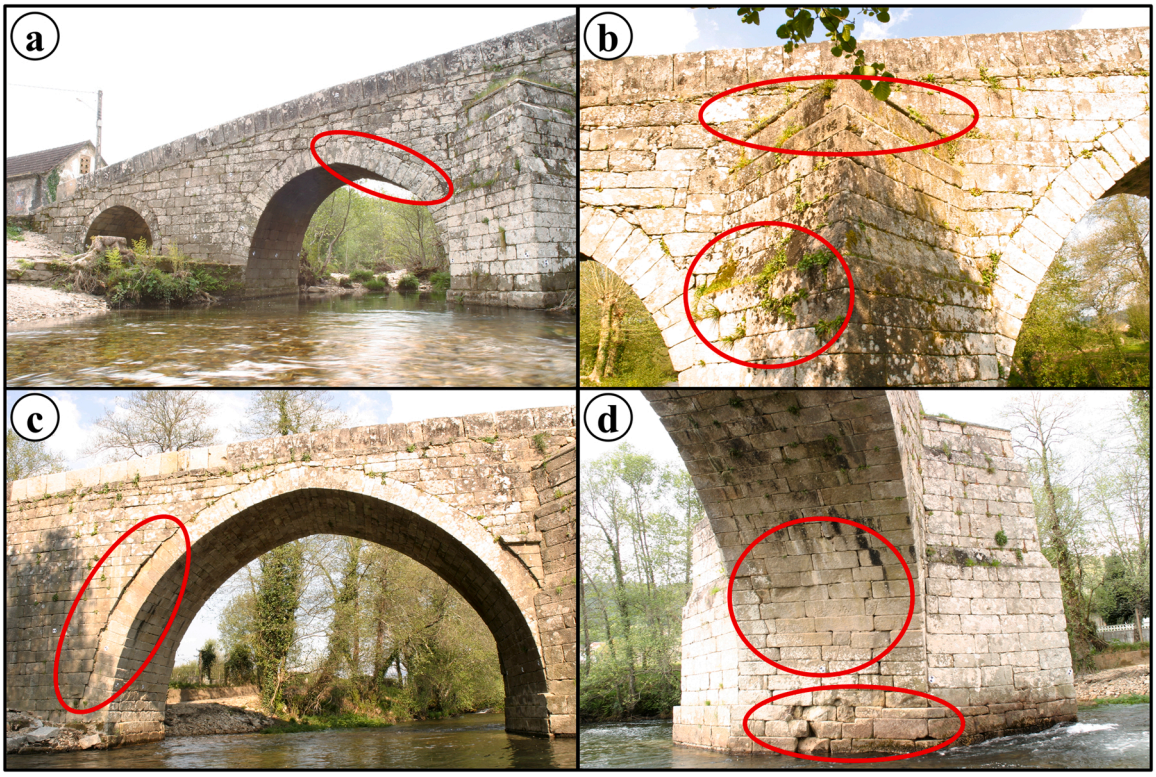

Fig. 3. Details of the current condition of Cernadela Bridge: (a) Deformation in arch D (b) Vegetation (c) Out-of-plane spandrel wall deformations (d) Cracks and detachment of elements.

2.3. Experimental campaign

2.3.1. TLS survey

In historical structures, there is usually a lack of information regarding geometrical dimensions in the form of, e.g., design drawings. Over the last few years, this issue has been overcome by using Terrestrial Laser Scanner (TLS) technology. The TLS is widely used in civil engineering to capture thousands of measuring points in a short period. Thus, the measuring points can be merged in a global point cloud, providing an accurate 3D digitalization of the whole construction.

In the case of the Cernadela Bridge, a TLS survey employing a Riegl LMS Z-390i 3D laser scanner was conducted. A scan project planning was developed to determine the scan positions, resolution, and the strategy to cope with the potential occlusions. Accordingly, twenty scans were recorded from ten different positions (Fig. 4). Additionally, twelve images were captured using a calibrated Nikon D2000 camera to record the color information of the construction. During the acquisition stage, a total station Leica TCR 307,

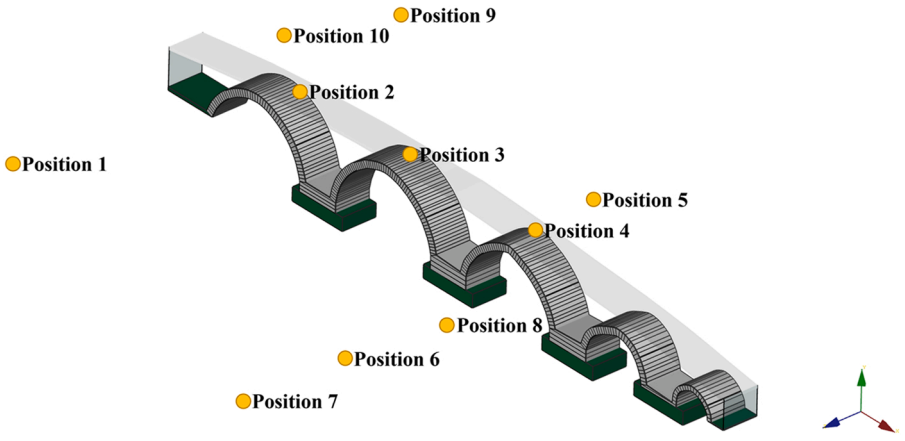

Fig. 4. Scheme of the laser scan positions.

was further used for leveling the captured point clouds, easing the subsequent registration in a common coordinate system. For this aim, several targets were distributed on the surface of the bridge. Finally, all laser scans were post-processed to obtain the downstream, upstream, and top view orthoimages, which provide a detailed geometric description of the entire bridge and its structural elements. The scan project planning, acquisition stage, and post-processing were deeply discussed in [27], where the interested reader might refer for further details.

2.3.2. GPR survey

Similar to the outer geometry, no information about the inner geometry is usually available in historic MABs. Hence, to geometrically characterize the inner parts (infill and backing) and pavement of the Cernadela Bridge, a Ground Penetrating Radar (GPR) survey was conducted. This sensor is well-known in civil engineering for its ability to generate radargrams of the subsurface through the propagation and reflection of short electromagnetic pulses defined by Maxwell's equations.

In the case of the Cernadela Bridge, a RAMAC/GPR system from MALÅ Geoscience was employed during the experimental campaign. Initially, a 500 MHz antenna was used to measure the inner bridge geometry, which consisted of conducting two longitudinal parallel lines in opposite directions through the bridge pathway, with a one-meter distance between them. An odometer wheel was attached to the antenna to control the trace distance while providing the profile lengths to facilitate positioning. However, in complex structures, the arches' thickness is not easily identified due to the heterogeneity of the fill materials and the possible irregularities in the fill-granite interface [28]. Therefore, to avoid these inconveniences, additional measurements were acquired using an 800 MHz antenna, which provides higher spatial resolution. In this case, the inner geometry was captured on three parallel lines conducted in the longitudinal direction through the internal surface of the arch vault. All the measurements were then filtered to obtain more accurate radargrams, which were corrected for topography considering the outer arches geometry captured by the TLS. The TLS data was also used to estimate the velocity of propagation of the GPR signal in granite stone, resulting in 12.0 cm/ns, thus allowing us to convert the travel-time distance in the radargrams into depth (thickness) values. Further details of the employed equipment, acquisition process and setting parameters, velocity estimation, and post-processing steps can be found in [29].

3. Structural assessment

3.1. Uncertainty quantification

When assessing heritage constructions, uncertainties in structural parameters must be considered to perform a reliable structural system performance evaluation. Uncertainties can be represented through random variables defined by Probability Density Functions (PDFs). However, it should be kept in mind that the proper definition of these distributions is critical due to their considerable influence on the reliability analysis results. Hence, to correctly define the distribution types and their parameters, available experimental data and recommendations provided in the existing literature must be studied thoroughly.

In this study, fourteen parameters were considered for the reliability-based structural assessment of the Cernadela Bridge. Regarding the geometrical parameters, the uncertainty definition was described using the experimentally obtained data. Thus, for the bridge width, sixty-five equidistant values were measured from the top view orthoimage (see Fig. 5). These measurements were then statistically processed by fitting a Normal distribution and verifying its adequacy by proper hypothesis testing procedures (i.e., Chi-Square Goodness-of-Fit and Anderson-Darling tests). As a result, the bridge width scattering was defined as a Normal distribution with a mean value of 3.38 m and a CoV (Coefficient of Variation) of 1.24 %.

Similarly, the variability of the voussoirs' dimensions in each arch was defined from the experimental measurements. In this case, using the downstream orthoimage, the external thickness values of the joints between voussoirs were measured individually (see Fig. 6). This way, between twenty and sixty experimental values per arch were extracted. Subsequently, each data cluster was

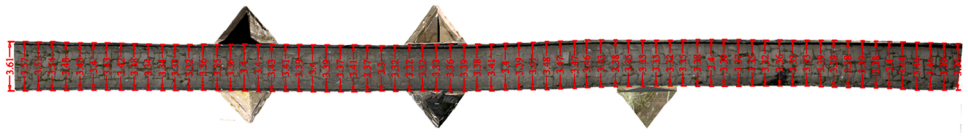

Fig. 5. Cernadela bridge width and detailing of the experimental measurements taken in the top view orthoimage.

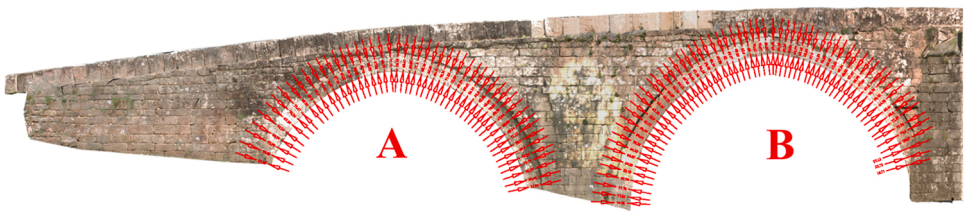

Fig. 6. Experimental measurement of the arches' outer thicknesses.

statistically processed and fitted to a Normal probability distribution whose parameters can be consulted in Table 1.

As for the internal geometrical properties of the bridge, the GPR results, which measure the depth of the different construction layers, were used to quantify the pavement thickness and backing height variability. As for the pavement, GPR measured depth and element thickness are equivalent; thus, the GPR profile data could be statistically processed directly. However, concerning the backing, no direct correlation exists between experimental measurements and backing heights. Thus, to transform the former measurements into values of the latter parameter, both the GPR profile and the downstream orthoimage were divided into six sections, one per pier or abutment. In each orthoimage section, between fifteen and twenty equidistant reference positions were defined, and their coordinates X_{ortho} were measured. Subsequently, the equivalent coordinates X_{GPR} were extracted in the GPR profile. As a result, the backfill depths could be derived in the equivalent slices of the GPR profile (see Fig. 7) and, from them, the backing heights.

It should be noted that both the backing height and the pavement thickness were modeled as a single stochastic variable. Experimental results showed significant variability in these two parameters over the bridge; thus, in both cases, a subjective description was introduced in the form of triangular probability distributions. On the one hand, the pavement thickness distribution was defined using the maximum and minimum experimentally obtained thicknesses as bound values and the mode of the measurements as the mode value. On the other hand, some previous issues were considered for the backing height. Accordingly, the values from Section 6 were disregarded due to their limited influence on the global mechanical response of the bridge. Thus, similarly to the pavement thickness, the backing height was defined as a triangular distribution based on the statistical processing of the measurements from the remaining sections. The statistical parameters of the triangular distributions for both stochastic variables can be consulted in Table 1.

As for the constituent materials, uncertainties were defined according to the recommendations provided in the existing literature. Accordingly, the probability distribution of the masonry's density was defined as a Normal distribution with a mean value of 2100 kg/m3 and a CoV of 5 % [30–32]. A log-normal PDF with a mean value of 3.0 MPa and a CoV of 20 % was adopted for the compressive strength [9,32,33]. The friction coefficient was defined as a log-normal distribution with a mean value of 0.58 and a CoV of 20 % [9,33]. Concerning the infill material, the density was represented by a Normal PDF with a mean value of 1800 kg/m3 and a CoV of 5 % [31,33], the cohesion by a log-normal distribution with a mean value of 20 kPa and a CoV of 30 % [4,33,34], and a Normal distribution with a mean value of 30.00 and a CoV of 10 % was adopted for the friction angle [33–35]. Table 1 summarizes all considered random variables indicating their distribution type and statistical moments.

3.2. Limit analysis model

The limit analysis method is an approach to calculating the ultimate limit state concerning the transformation of the structure, or a part of it, into a mechanism that leads to collapse. It was initially developed for steel components and structures. Posteriorly, Heyman [36] and Pippard [37] adapted it to single unreinforced masonry arches by considering the following hypothesis: (i) there is no tensile strength between masonry blocks, (ii) masonry has infinite compressive strength, and (iii) no sliding between masonry blocks can occur. Recently, Gilbert [38] extended the scope of the method to calculate sliding between adjacent blocks, finite masonry strength, multi-span bridges, multi-ring arches, and reinforced masonry arches.

In this paper, the Limit State's software RING version 3.2.c was used to perform the calculations. Within RING, a masonry bridge is represented as a two-dimensional structural model where the arches are idealized as a series of blocks separated by frictional-contact

Table 1
Uncertain structural parameters of Cernadela Bridge.

ID	Parameter	Distribution type	μ	σ
V1	Arch A thickness	Normal	68.63 cm	3.85 cm
V2	Arch B thickness	Normal	65.76 cm	4.26 cm
V3	Arch C thickness	Normal	63.13 cm	4.76 cm
V4	Arch D thickness	Normal	64.31 cm	4.88 cm
V5	Arch E thickness	Normal	41.82 cm	2.90 cm
V6	Bridge width	Normal	3.38 m	0.04 m
V7	Pavement thickness	Triangular	32.75 cm	5.82 cm
V8	Backing height	Triangular	2.67 m	0.43 m
V9	Masonry density	Normal	2100 kg/m^3	105.00 kg/m^3
V10	Masonry compressive strength	Log-normal	3.00 MPa	0.60 MPa
V11	Masonry friction coefficient	Log-normal	0.58	0.12
V12	Backfill density	Normal	1800 kg/m^3	90.00 kg/m^3
V13	Backfill cohesion	Log-normal	20.00 kPa	6.00 kPa
V14	Backfill friction angle	Normal	30.00	3.00

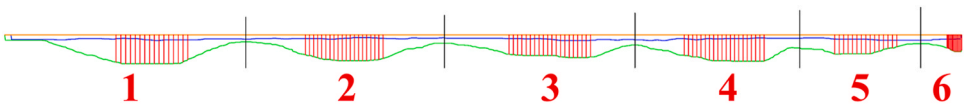

Fig. 7. GPR profile measuring the backfill depth at different bridge sections.

interfaces. Thus, transverse effects, which may affect the strength capacity [4,39,40], cannot be considered. The fill material is not explicitly modeled but considered indirectly through the effect of its dead weight, the dispersion of live loads, and the mobilization of passive earth pressures. In this regard, the lateral backfill forces are modeled using compression-only one-dimensional elements, with maximum values limited to avoid sliding of the backfill at the interface with the arch. The model can predict the failure of masonry structures due to the formation of plastic hinges or sliding planes that transform the structure into a mechanism. To estimate the ultimate load-carrying capacity of the structure, RING uses a linear programming optimization technique to compute the ultimate load factor, the corresponding critical loading position, and the associated collapse mechanism (i.e., the position of the plastic hinges or sliding planes).

The data gathered from the experimental characterization campaign were used to build the limit analysis computational model (see Fig. 8). Accordingly, the geometry of the different bridge elements was extracted from the orthoimages. Thus, the slope of the pavement was defined through the coordinates of twenty-seven points measured in the downstream orthoimage. Similarly, the number and position of the different voussoirs were accurately represented by measuring their intrados coordinates. The same approach was used to introduce the piers' geometry. As for the foundations and the soil, no geotechnical data was available. Thus, no possible scour-induced damage [41] was considered in the model. The live load dispersion through the infill was modeled according to the Boussinesq distribution model with an angle of 30º. In the transversal direction, the effective bridge width was considered equal to the geometric width. For the calculation of the limit load of the structure, the roadway traffic load model LM1, established in the standard EN 1991–2 [42], was adopted. The LM1 load model is characterized by two axles of 2.0 m width each, separated by a distance of 1.2 m and a load of 300 kN per axle. A total of one hundred loading positions were defined, with a spacing of 0.6 m along the bridge deck.

Initially, a deterministic analysis assuming the mean values in Table 1 for geometrical and material properties was performed to determine the ultimate load and critical loading position. Fig. 9 illustrates the received collapse mechanism. The failure is triggered due to the formation of a four hinges mechanism in arch C. An ultimate load factor of 2.23 was obtained, which seems to indicate that the roadway traffic might safely cross the bridge. However, it should be noted that these results correspond to the ultimate strength of the bridge evaluated considering loading effects mainly along the span length, thus disregarding any possible transverse weakness induced by the action of out-of-plane effects. Furthermore, a more qualified reliability analysis considering parameters uncertainties shall be performed to draw a more rigorous judgment, which will be addressed in the following sections.

3.3. Reliability analysis

Any structure must fulfill specific requirements during its lifetime. In reliability analyses, these requirements are expressed through limit states that delimit the safe and unsafe regions regarding the target system performance. The limit states can refer to the serviceability and functionality of the structure (Serviceability Limit State) or strength and stability requirements (Ultimate Limit State). For instance, the Ultimate Limit State (ULS) related to the collapse of the bridge due to its transformation, or a part of it, into a mechanism can be mathematically represented as a function $g(\boldsymbol{X})$, where $\boldsymbol{X}$ is a vector of random variables, comparing the resistance R and the effects of loads S:

$$g(\boldsymbol{X}) = R - S \tag{1}$$

Thus, the probability of failure p_f can be defined as:

$$p_f = P(g(\boldsymbol{X}) \leq 0) = P(R \leq S) \tag{2}$$

An alternative indicator, the reliability index β [43], which denotes the reliability level of the structure, can also be defined as:

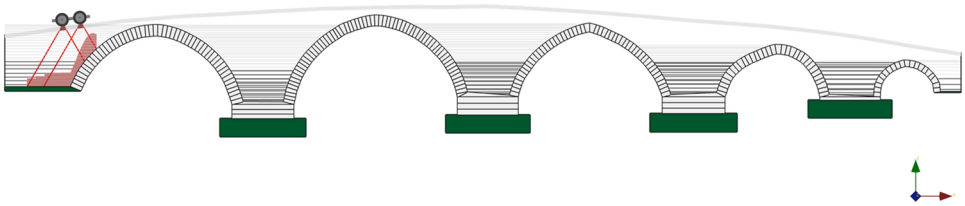

Fig. 8. Limit analysis model of Cernadela Bridge.

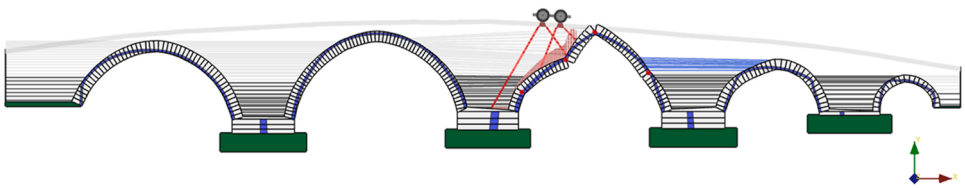

Fig. 9. Collapse mechanism of the Cernadela bridge obtained in the deterministic analysis.

$$\beta = -\Phi^{-1}(p_f) \tag{3}$$

where $\Phi(\bullet)$ is the standard normal cumulative distribution function.

In order to assess bridge safety, reliability analyses shall be performed to obtain the reliability indexes, which shall be compared with the target values established in the current standards. In this paper, the reliability analysis procedure presented by Galvão et al. [44], Moreira et al. [9,15] and Matos et al. [14,45] was adopted. Thus, the load curve *S* defines the uncertainties related to loading values, which were modeled using a Gumbel distribution with a CoV of 15 %, considering a 95th percentile and a return period of 50 years, and only the concentrated forces, as suggested in [16]. The resultant loading PDF is shown in Table 2.

On the other hand, the resistance curve *R* was obtained based on a sampling process. Thus, a total of 100 points were generated by sampling the probability distributions in Table 1 through a Latin Hypercube Sampling (LHS) technique. Each sample describes a set of parameter values introduced in the structural model that provide the ultimate load factor, the critical loading position, and the collapse mechanism. These results showed that almost three-fourths (71 %) of the collapse mechanisms corresponded to the four hinges mechanism, see Fig. 11. Nevertheless, different failure modes, such as sliding (17 %), eight hinges (6 %), and four hinges and sliding (6 %) collapse mechanisms, were also received for some sampling points, see Fig. 10. As for the critical loading position, most of them are placed on the central arches B (9 %) and C (90 %). The resistance curve *R* was defined by fitting a Normal distribution to the histogram of collapse load values (see Fig. 11) and verifying its adequacy by proper hypothesis testing procedures (i.e., Chi-Square Goodness-of-Fit and Anderson-Darling tests). The obtained resistance PDF is shown in Table 2. Finally, once both curves were defined, the reliability index β was calculated by simulation methods, yielding a value of 2.38.

Table 2
Resistance and effects of loads curves.

	Distribution type	μ	σ
Resistance model (***R***)	Normal	2.11	0.44
Effects of loads model (***S***)	Gumbel	1.00	0.15

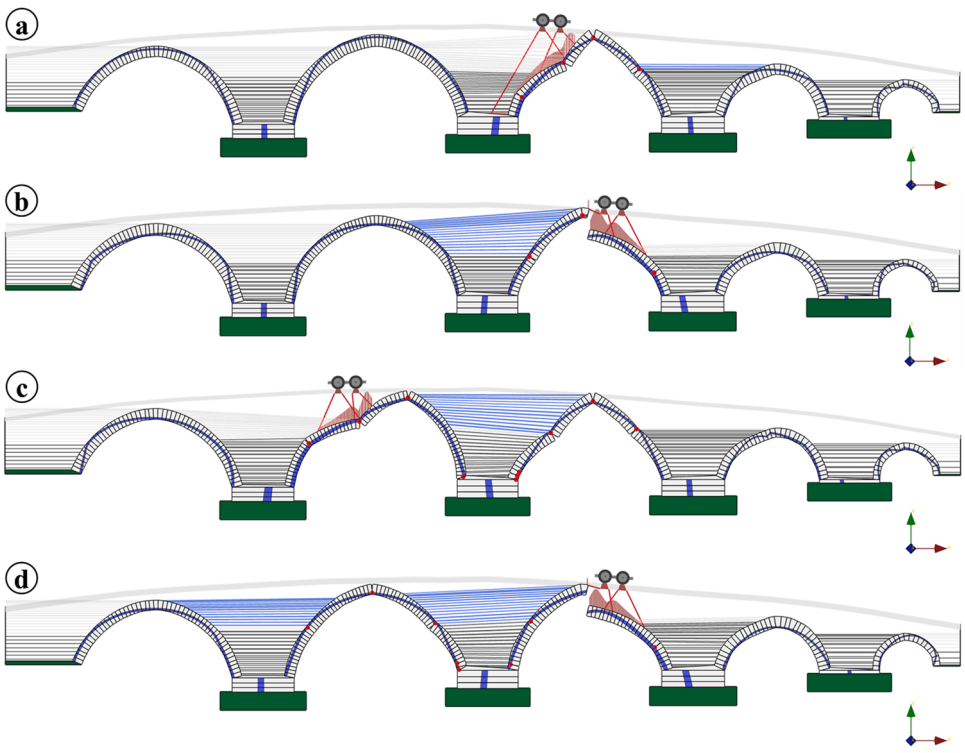

Fig. 10. Different collapse mechanisms of the Cernadela Bridge obtained in the stochastic analysis: (a) Four hinges collapse mechanism (b) Sliding collapse mechanism (c) Eight hinges collapse mechanism (d) Four hinges and sliding collapse mechanism.

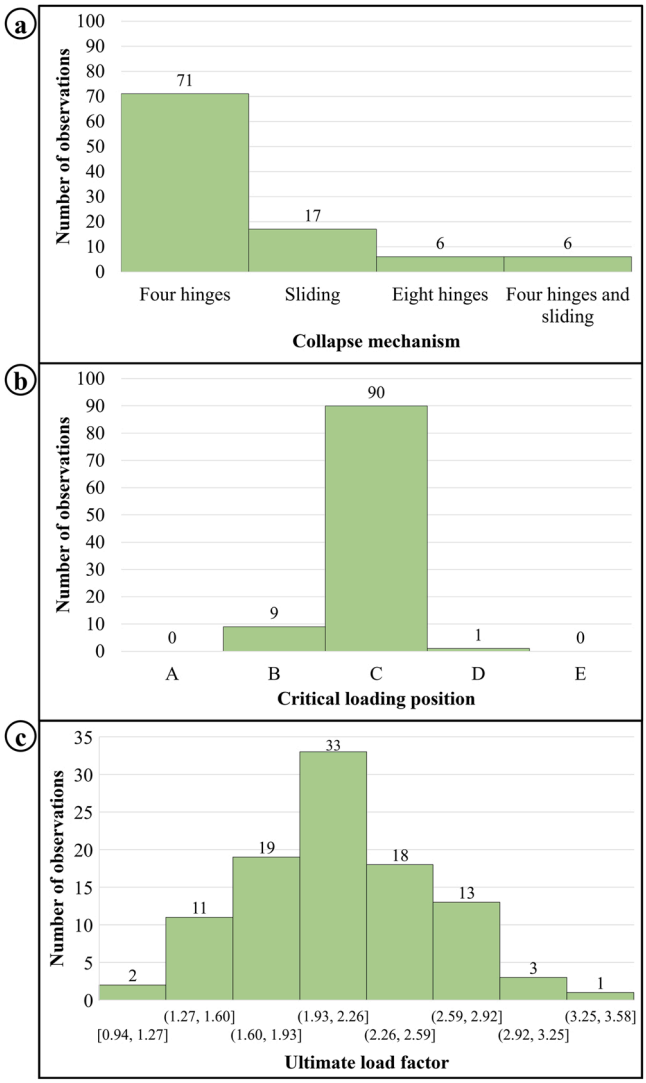

Fig. 11. Results of the stochastic analysis: (a) Distribution of the different collapse mechanisms (b) Distribution of the critical loading positions (c) Histogram of the ultimate load factors.

3.4. Safety assessment

In order to collect adequate target reliability indexes β_T, four different standards were consulted: UNE-EN 1990 [46], ISO 2394 [47], ISO 13822 [48], and JCSS Probabilistic Model Code (PMC) [30], which present differences that should be mentioned. Firstly, only the ISO 2394 and the ISO 13822 are referred to existing structures; the UNE-EN 1990 and the JCSS PMC establish target reliability indexes for designing new structures. ISO 2394 states that the target reliability indexes should be identical for new and existing structures. On the contrary, the JCSS PMC and the ISO 13822 point out that it cannot be possible due to the high social, economic, and sustainability costs of increasing the reliability level of an existing structure.

Additionally, each standard is referred to different reference periods. The target reliability indexes established by ISO 13822 are referred to the minimum standard period of safety (e.g., 50 years), while the JCSS PMC and ISO 2394 consider a one-year reference period. On the other hand, the UNE-EN 1990 specifies different indexes for reference periods of one and fifty years. All the target reliability indexes are defined according to the consequences of the failure of the structure. However, each standard has a different approach. In UNE-EN 1990, these consequences are classified according to the social, economic, living, and environmental costs that the collapse of the construction would provoke. On the other hand, ISO 2394 and ISO 13822 define the consequences through the calculation of the Life Quality Index (LQI), which allows the calculation of the life-saving costs and the money that shall be invested to save an additional life. Finally, the JCSS PMC classifies the consequences of failure attending the type of failure (e.g., a structure that may collapse suddenly shall be classified as a structure with large consequences of failure).

In this work, due to the reduced traffic and its limited width, yet its historical and heritage value, the Cernadela bridge has been classified as a structure with moderate consequences of failure. Regarding the life savings and safety costs, the expenses required for increasing the structure's reliability level are high because the bridge has already surpassed the design life (100 years). Consequently, the highest reliability index related to life-saving costs should be considered. Table 3 shows the selected target reliability indexes, the calculated reliability index, and their comparison. The results indicate that the Cernadela bridge does not present satisfactory structural performance to withstand roadway traffic loads safely. In this regard, it should be noted that the current mandatory load models far surpass the solicitations that the bridge actually withstands daily. Nonetheless, adequate rehabilitation works would be desired so as to assure the safety and preservation of the structure.

4. Sensitivity analysis

A global variance-based sensitivity analysis was conducted to obtain further insight into the bridge mechanical response by identifying the most influential structural parameters on the collapse load. The selected sensitivity analysis methodology (i.e., Sobol' indices) requires a substantial number of simulation runs and, consequently, a high computational cost. Thus, a surrogate model based on the Kriging approach was built to substitute the original limit analysis model, easing the analysis process and reducing the numerical effort while maintaining the accuracy of the results.

4.1. Surrogate modeling

The Kriging approach is a statistical interpolation method that allows approximating a scalar-valued response $\widehat{y}(\boldsymbol{x})$ for a vector of input parameter values $\boldsymbol{x}$. The functional relationship can be expressed by Eq. (4) [49].

$$\widehat{y}(\boldsymbol{x}) = \boldsymbol{f}(\boldsymbol{x})^T \bullet \boldsymbol{\beta} + Z(\boldsymbol{x}) \tag{4}$$

where the first term $\boldsymbol{f}(\boldsymbol{x})^T \bullet \boldsymbol{\beta}$ corresponds to the trend or mean value, consisting of P basis functions $\boldsymbol{f}(\boldsymbol{x}) = [\boldsymbol{f_1}(\boldsymbol{x}), \ldots, \boldsymbol{f_P}(\boldsymbol{x})]^T$ with their corresponding regression coefficients $\boldsymbol{\beta} = [\beta_1, \ldots, \beta_P]^T$. The second term $Z(\boldsymbol{x})$, represents a stationary random process with zero mean and covariance function of the form [50]:

$$Cov(\boldsymbol{x}, \boldsymbol{x}') = \sigma^2 \bullet R(\boldsymbol{x}, \boldsymbol{x}'; \boldsymbol{\theta}) \tag{5}$$

where σ^2 is the variance, $R(\boldsymbol{x}, \boldsymbol{x}'; \boldsymbol{\theta})$ is the correlation function and $\boldsymbol{\theta} = [\theta_1, \ldots, \theta_m]^T$ are hyperparameters that can be calculated through an optimization process.

In this study, a surrogate model for the ultimate load factor $\widehat{f_{UL}}$ was trained using the 100 LHS samples generated in the previous stochastic analysis. The forecasting capability was then assessed through the coefficient of determination R^2 and the Root-Mean Square Error *RMSE* metrics.

Table 3
Initial structural safety assessment results of the Cernadela Bridge.

Standard	Target reliability index (β_t)	Reliability index (β)
UNE-EN 1990	3.80	2.38
ISO 2394	3.10	
ISO 13822	3.80	
JCSS PMC	3.30	

$$R^2 = 1 - \frac{\sum_{i=1}^{n}(y_i - \widehat{y}_i)^2}{\sum_{i=1}^{n}(y_i - \overline{y})^2} \tag{6}$$

$$RMSE = \sqrt{\frac{1}{n}\sum_{i=1}^{n}(y_i - \widehat{y}_i)^2} \tag{7}$$

where y_i refers to the computational model response at the point i and $\widehat{y}_i$ corresponds to the associated surrogate model prediction. On the other hand, $\overline{y}$ denotes the average value of the model responses, and n is the total number of samples used during the training process. Accordingly, for the best-generated surrogate model, a coefficient of determination of 0.95 and a Root-Mean Square Error of 9.42E-02 were obtained. These results indicate that the approximation model accurately replicates the responses of the computational limit analysis model.

4.2. Variance-based sensitivity indices

Sobol' sensitivity indices quantify which percentage of the model output variance can be apportioned to each model input variable [51]. Thus, the output variance is expressed as the sum of the partial variances of each input parameter and their interaction effects. According to [52], in general terms, the sensitivity $S_{i_1,\ldots,i_S}$ can be expressed as the variance contribution $V_{i_1,\ldots,i_S}$ of a set of input parameters $\{X_{i_1,\ldots,i_S}\}$ to the total output variance $V(Y)$.

$$S_{i_1,\ldots,i_S} = \frac{V_{i_1,\ldots,i_S}}{V(Y)} \tag{8}$$

On the one hand, the first-order Sobol' index (S_i) quantifies the contribution to the total model output variance $V(Y)$ of each input variable individually.

$$S_i = \frac{V_i}{V(Y)} \tag{9}$$

On the other hand, the total Sobol' index (S_{Ti}) quantifies not only the output variance caused by the individual contribution of a given input variable but also from all its possible interactions, which is calculated through the summation of the first-order S_i and higher-order Sobol' indices $S_{i,\sim i}$.

$$S_{Ti} = S_i + S_{i,\sim i} = \frac{V_i + V_{i,\sim i}}{V(Y)} \tag{10}$$

where V_i represents the individual effect of each input parameter, and $V_{i,\sim i}$ the interaction effects with all other variables.

In this work, the influence of the uncertain structural parameters given in Table 1 on the ultimate load factor of the bridge was analyzed. To perform the sensitivity analysis, a total of 100,000 samples were generated through LHS sampling, and for each, the surrogate model was exercised to calculate the ultimate load factor. Fig. 12 shows the obtained first-order and total Sobol' sensitivity indices. A threshold value of 5.00 % was established so as to deem a parameter as influential. Out of the fourteen variables, only three have a noticeable influence on the ultimate load factor: the thickness of arch C, the masonry compressive strength, and the friction coefficient. Thus, it can be concluded that the most critical parameter is the arch C thickness, which accounts for approximately 50 % of the variance of the model output. This considerable influence can be explained by the location of the most critical loading positions and the received collapse mechanisms, as shown in Fig. 11. Besides, the results confirm the critical importance of accurately defining the uncertainties regarding the geometry of the arches, particularly with respect to the joints thickness dimensions. Hence, in the

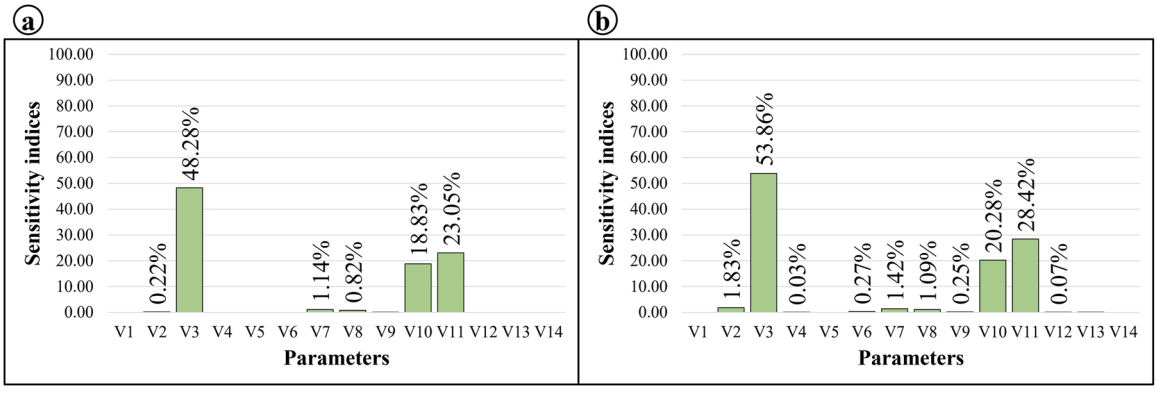

Fig. 12. Sensitivity analysis results: (a) First Order Sobol' indices (b) Total Sobol' indices.

following, a Bayesian inference process will be performed to update the prior PDFs associated with these parameters and thus reduce their statistical uncertainty.

5. Bayesian inference

5.1. Updating the prior probabilistic model

Bayesian inference is a statistical procedure that allows updating the prior probability distributions by introducing new data, such as experimental results or observations, leading to a decrease in the statistical uncertainty of the random variables' parameters. The updating process is based on the Bayes theorem, which weights the prior distributions and the likelihood (i.e., the experimental data) to yield the posterior distributions, summarizing all the existing and collected information.

In this work, Bayesian inference was used to update the PDFs of the thickness of all arches, introducing the measurements regarding internal geometry. A Normal likelihood and conjugate prior distributions were assumed during the updating process. As for the likelihood, the experimental data from the GPR campaign was statistically processed, fitted to normal distributions, and appropriately verified by a hypothesis testing procedure, particularly by the Chi-Square Goodness-of-Fit and the Anderson-Darling tests. Concerning the prior distributions, informative prior distributions were used, which allow for considering the previous information, in this case, regarding the external geometry gathered from the TLS. The adopted Bayesian framework is described in the following for the case when both statistical moments μ and σ^2 are unknown. For conciseness, the framework is exemplified for updating the random variable describing the thickness of arch C.

The conjugate prior of a normal distribution with unknown mean and variance is a normal-inverse-gamma distribution:

$$p(\mu,\sigma^2) \sim NIG\left(\mu_0, \frac{\sigma^2}{n_0}; \frac{v_0}{2}, \frac{v_0}{2}\sigma_0^2\right) \tag{11}$$

where n_0 denotes the prior sample size, μ_0 and σ_0^2 are the mean and the variance, and $v_0 = n_0 - 1$ corresponds to the degrees of freedom. In this case, $n_0 = 30$ (the same weight is given to the prior and the likelihood data), $\mu_0 = 63.13$, and $\sigma_0^2 = 22.66$.

The joint prior density can alternatively be expressed as the product of a conditional probability and a marginal probability, as in Eq. (12).

$$p(\mu|\sigma^2) = p(\mu|\sigma^2) \bullet p(\sigma^2) \tag{12}$$

where $p(\mu|\sigma^2)$, the prior conditional distribution of μ given σ^2, is a Normal distribution with mean μ_0 and variance σ^2/n_0:

$$\mu|\sigma^2 \sim N\left(\mu_0; \frac{\sigma^2}{n_0}\right) \rightarrow \mu|\sigma^2 \sim N\left(63.13; \frac{\sigma^2}{30}\right) \tag{13}$$

and $p(\sigma^2)$, the marginal prior distribution of σ^2, is an inverse gamma distribution with shape $\alpha_0 = v_0/2$ and scale $\beta_0 = (v_0/2) \bullet \sigma_0^2$:

$$\sigma^2 \sim IG(\alpha_0, \beta_0) \rightarrow \sigma^2 \sim IG(14.50, 328.53) \tag{14}$$

Considering the experimental data $y = \{y_1, \ldots, y_n\}$, which for arch C has numerical summaries $\bar{y} = 62.93$ (sample mean), $s^2 = 214.92$ (sample variance), and $n = 30$ (number of test results), the conditional posterior distribution of μ given σ^2 is also a Normal distribution with mean μ_n and variance σ^2/n_n:

$$\mu\left|\sigma^2, y \sim N\left(\mu_n; \frac{\sigma^2}{n_n}\right) \rightarrow \mu\right|\sigma^2, y \sim N\left(63.03; \frac{\sigma^2}{60}\right) \tag{15}$$

where

$$\mu_n = \frac{n_0}{n_0 + n} \bullet \mu_0 + \frac{n}{n_0 + n} \bullet \bar{y}$$

$$n_n = n_0 + n$$

The posterior distribution parameters combine the prior distribution information and the one contained in the experimental data. Thus, μ_n is a weighted average of the prior μ_0 and sample mean $\bar{y}$, with weights determined by the relative precision of the two pieces of information [53].

The marginal posterior distribution of σ^2 is an inverse gamma distribution with updated hyperparameters $\alpha_n = v_n/2$ and $\beta_n = (v_n/2) \bullet \sigma_n^2$:

$$\sigma^2|y \sim IG(\alpha_n, \beta_n) \rightarrow \sigma^2|y \sim IG(29.50, 3445.11) \tag{16}$$

where:

$$v_n = v_0 + n$$

$$v_n\sigma_n^2 = v_0\sigma_0^2 + (n-1)\bullet s^2 + \frac{n_0 \bullet n}{n_0 + n}\bullet(\bar{y}-\mu_0)^2$$

The posterior sum of squares $v_n\sigma_n^2$, combines the prior $v_0\sigma_0^2$ and the sample $(n-1)\bullet s^2$ sum of squares, with the additional uncertainty given by the difference between the prior and the sample mean [53]. To calculate the posterior distribution of the parameters, analytical expressions or simulation methods using Eqs. (15) and (16) can be used [53].

Table 4 provides the results for the posterior distributions obtained from the Bayesian analysis regarding the thickness of arch C. Fig. 13 shows, together with the prior distribution and the likelihood function, a plot of the resulting posterior distribution of the population. Finally, Table 5 summarizes the distribution types and corresponding statistical moments for all random variables

Table 4
Posterior distribution parameters values for the thickness of arch C.

Parameter	Posterior
μ_0	63.13
σ_0	4.76
μ	63.03
$\sigma(\mu)$	1.42
σ	10.95
$\sigma(\sigma)$	1.03
μ_{pop}	63.03
σ_{pop}	11.09

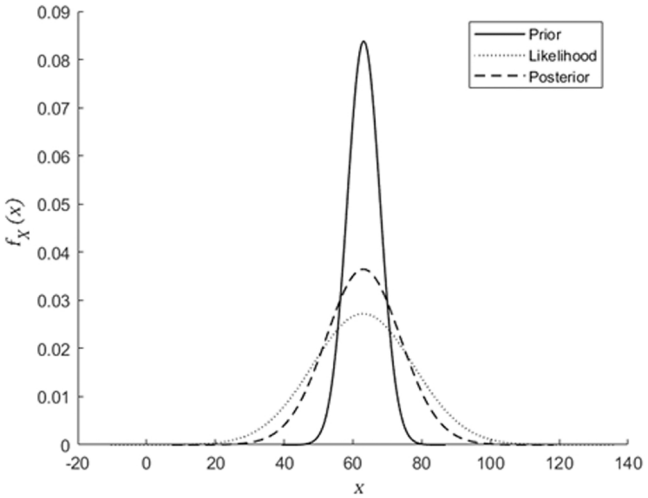

Fig. 13. Prior and posterior probability density functions after Bayesian inference (arch C thickness).

Table 5
Random variables after Bayesian inference.

ID	Parameter	Distribution type	μ	σ
VP1	Arch A thickness	Normal	62.10 cm	9.45 cm
VP2	Arch B thickness	Normal	60.62 cm	8.20 cm
VP3	Arch C thickness	Normal	63.03 cm	11.09 cm
VP4	Arch D thickness	Normal	61.69 cm	6.46 cm
VP5	Arch E thickness	Normal	41.86 cm	4.13 cm
VP6	Bridge width	Normal	3.38 m	0.04 m
VP7	Pavement thickness	Triangular	32.75 cm	5.82 cm
VP8	Backing height	Triangular	2.67 m	0.43 m
VP9	Masonry density	Normal	2100 kg/m^3	105.00 kg/m^3
VP10	Masonry compressive strength	Log-normal	3.00 MPa	0.60 MPa
VP11	Masonry friction coefficient	Log-normal	0.58	0.12
VP12	Backfill density	Normal	1800 kg/m^3	90.00 kg/m^3
VP13	Backfill cohesion	Log-normal	20.00 kPa	6.00 kPa
VP14	Backfill friction angle	Normal	30.00	3.00

considered in the reliability analysis.

5.2. Reliability analysis based on Bayesian updating results

In order to study the effect of the updated parameters (i.e., the thickness of the arches), two additional reliability analyses were performed.

Firstly, the ultimate load-carrying capacity of the bridge was determined using the updated PDFs of all the arches' thicknesses. For that purpose, 100 new LHS samples were generated. Each set of input values was introduced in the limit analysis model computing the ultimate load factor, critical loading position, and collapse mechanism. Significant differences were found regarding the former sampling results. The number of collapse mechanisms involving four hinges slightly increased (83 %), while the mechanisms concerning sliding (6 %) and the combination of sliding with four hinges decreased (4 %). Additionally, the percentage of eight hinges collapse mechanisms remained almost invariable (6 %). Concerning the critical loading position, the most unfavorable section was located again on arch C (51 %). However, for an important number of sampling points, the critical loading position was also placed on arches B (26 %), A (17 %), and D (5 %). As for the ultimate load factor, an average value of 1.81 was calculated, which clearly shows how the prior distributions overestimate the thicknesses of the arches and, consequently, the ultimate load of the bridge. From the new histogram of ultimate load factors (see Fig. 14), a Normal PDF was fitted to define the resistance curve R_1 (see Table 6), which allows for deriving the updated reliability index β_1, see Table 7.

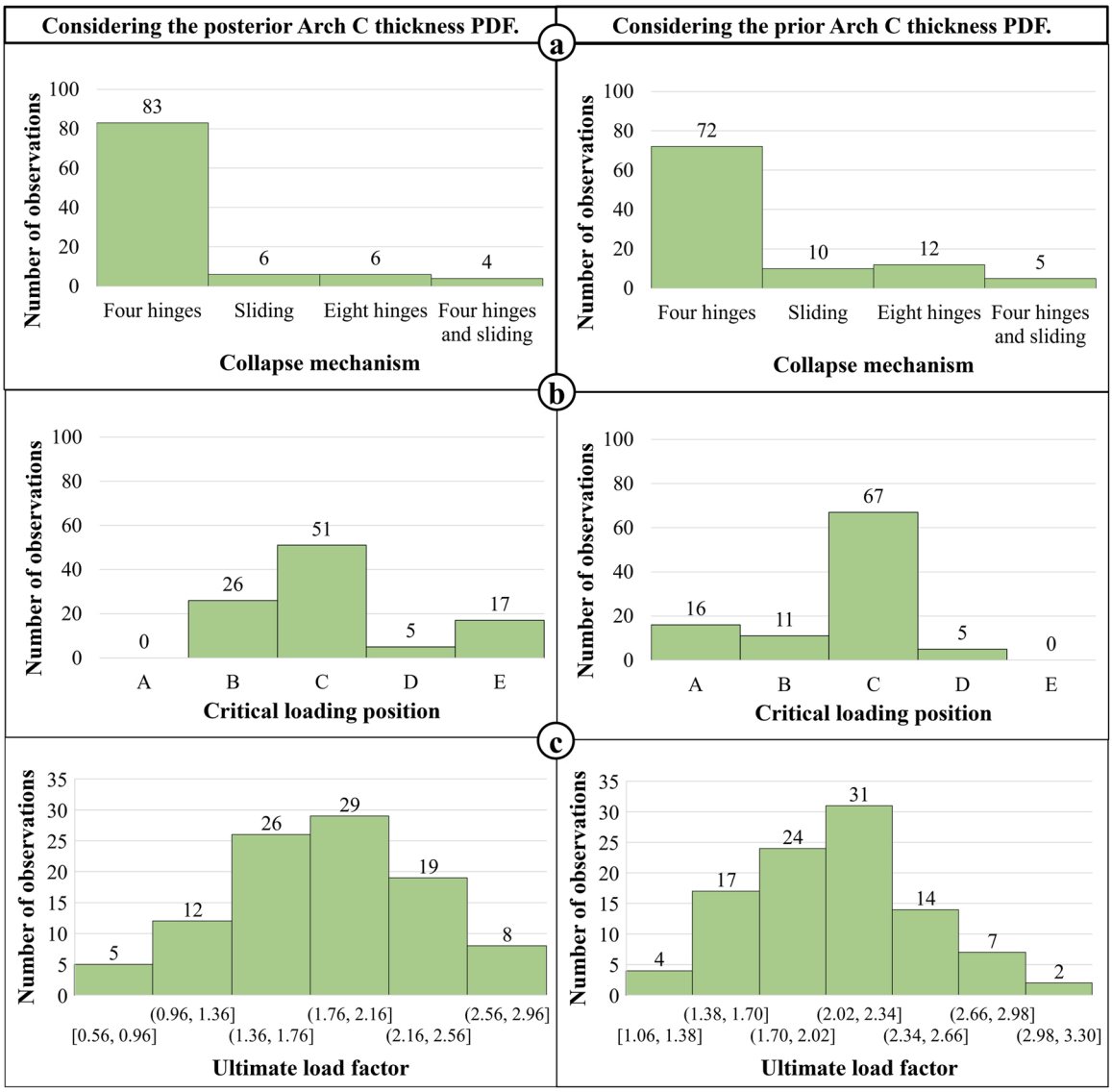

Fig. 14. Results of the stochastic analysis after Bayesian updating: (a) Distribution of the different collapse mechanisms (b) Distribution of the critical loading positions (c) Histogram of the ultimate load factors.

Table 6
Resistance and effects of loads curves after Bayesian updating.

	Distribution type	μ	σ
Resistance model: all arches thicknesses updated ($\boldsymbol{R_1}$)	Normal	1.82	0.52
Resistance model: non-influential arches thicknesses updated ($\boldsymbol{R_2}$)	Normal	2.04	0.42
Effects of loads model ($\boldsymbol{S}$)	Gumbel	1.00	0.15

Table 7
Structural safety assessment results of the Cernadela Bridge after Bayesian updating.

Standard	Target reliability index (β_t)	Reliability index: all arches thicknesses updated (β_1)	Reliability index: non-influential arches thicknesses updated (β_2)
UNE-EN 1990	3.80	1.51	2.33
ISO 2394	3.10		
ISO 13822	3.80		
JCSS PMC	3.30		

Secondly, the previous analysis procedure was repeated but considering the prior distribution for the most influential parameters (i.e., the thickness of arch C). The results showed high similitude with the initial reliability analysis performed with the prior distribution of all parameters. Indeed, almost no variability was observed for the ultimate load factor, obtaining an average value of 2.05. These results clearly underline the importance of the sensitivity analysis studies so as to gain a better understating of the impact of the different uncertain structural parameters on the collapse load estimation of the structure. As for the collapse mechanisms, almost three-fourths (72 %) corresponded to the four hinges collapse mechanism, while minor differences in sliding (10 %), eight hinges (12 %), and four hinges and sliding (5 %) collapse mechanisms were observed. Besides, some differences also arise concerning the critical loading position. Initially, most of the critical loads were placed on arches B and C. In this analysis, much more distributed positions were obtained: 67 % on arch C, 16 % on arch A, 11 % on arch B, and 5 % on arch D. Finally, the resistance curve R_2 (see Table 6) was fitted to the histogram of ultimate load factors (see Fig. 14), and the reliability index β_2 computed, see Table 7.

In Table 7, all the calculated reliability indexes are given. Three main conclusions can be extracted from the results: (i) the accuracy of the reliability-based assessment is significantly dependent on the appropriateness of the uncertainty quantification process; in this study, there is an apparent overestimation of the ultimate load-carrying capacity of the Cernadela bridge when the internal voussoirs' geometry is neglected; (ii) sensitivity analysis allows identifying the critical structural parameters, i.e., those major impacting the bridge strength, and therefore those on which experimental characterization tests should be primarily focused so as to reduce uncertainty; (iii) the Cernadela Bridge does not present satisfactory structural performance to withstand roadway traffic loads safely. Hence, the passage of cars should be seen as an exceptional situation; otherwise, structural strengthening and retrofitting works should be accomplished.

6. Conclusions

This paper addressed the geometrical characterization through geomatic techniques (terrestrial laser scanning and ground penetrating radar) and probabilistic-based structural safety assessment of the Cernadela bridge, a medieval stone arch bridge in Galicia, northwest Spain. The following conclusions can be drawn from the study:

- In masonry bridges, voussoirs dimensions are typically a critical parameter for the determination of the ultimate load-carrying capacity of the structure. These elements usually present significant scattering between the outer ring and the inner parts. Considering only the former leads to an overestimation of the actual dimensions and, consequently, an overestimation of the bridge's load capacity. Thus, the probabilistic model of these parameters should be based on both inner and outer dimensions. This process can be performed by initially characterizing the uncertainties based on the outer (visible) data and, subsequently, updating the distributions using additional experimental measurements of the inner geometry through Bayesian inference procedures.
- An inaccurate uncertainty quantification process might lead to non-reliable assessment results. This study performed several reliability-based structural evaluations of the same bridge. Initially, only the voussoirs' outer dimensions were considered for defining the arches' ring thicknesses in the limit analysis model. Subsequently, Bayesian inference procedures introduced the experimentally obtained geometrical inner data in the probabilistic model. A difference of 36.55 % between reliability indexes was obtained, thus highlighting the importance of correctly characterizing the probability distributions of the structural parameters.
- The parameters that have more influence on the assessed outputs are the main contributors to the potential inaccuracies in the evaluation results. These parameters can be identified based on a sensitivity analysis. In this study, Sobol' indices were calculated by resorting to a surrogate-assisted sensitivity analysis strategy, pointing out that the critical parameter was the thickness of arch C. Thus, two different reliability-based assessments were performed. In the former, the updated probability distributions of all the arches' thicknesses were considered, and a difference of 36.55 % regarding the initial reliability assessment results was obtained. In the latter, the prior distribution for the thickness of arch C was kept, yielding a difference of 2.10 % regarding the initial assessment results. Thus the relevance of sensitivity analysis is stressed since they help not only to detect those parameters on which

experimental characterization tests should be primarily focused to reduce uncertainty but also to understand the underlying bridge mechanics better.

- Concerning the Cernadela bridge, the outputs from the reliability-based structural assessments allow us to conclude that the bridge does not present satisfactory structural performance to withstand road traffic loads safely. Therefore, the passage of cars should be seen as an exceptional situation; otherwise, strengthening and retrofitting works should be accomplished.

Future works will focus on improving the proposed methodology by considering additional aspects such as transverse (out-of-plane) and scouring effects. Regarding the former, three-dimensional modeling approaches such as those based on FEM (Finite Element Method) or DEM (Discrete Element Method) shall be used. As for scouring, an experimental geotechnical campaign should be performed to obtain the required foundation and soil data. This information may be introduced in the reliability-based assessment procedure by defining different scour scenarios. The scour damage might be considered by introducing translational springs at the piers and abutments of the numerical model that simulate the soil-structure interaction.

Declaration of Competing Interest

The authors declare that they have no known competing financial interests or personal relationships that could have appeared to influence the work reported in this paper.

Data Availability

The authors do not have permission to share data.

Acknowledgments

This work has been partially supported by the Spanish Ministry of Science and Innovation through the project Ref. TED2021-130497A-I00. This work has also received funding from the European Union's Horizon 2020 research and innovation program under Grant Agreement No 958171. This document reflects only the views of the author(s). Neither the Innovation and Networks Executive Agency (INEA) nor the European Commission is in any way responsible for any use that may be made of the information it contains. M. Solla acknowledges the grant RYC2019-026604-I funded by MCIN/AEI/10.13039/501100011033 and by "ESF Investing in your future." O. Bouzas acknowledges the human resources grant: "Axudas para a contratación de personal investigador predoutoral en formacion da Universidade De Vigo 2022" (PREUVIGO-22) funded by Universidade de Vigo.

References

[1] V. Sarhosis, S. de Santis, G. de Felice, A review of experimental investigations and assessment methods for masonry arch bridges, Struct. Infrastruct. Eng. 12 (2016) 1439–1464, https://doi.org/10.1080/15732479.2015.1136655.
[2] Pippard A.J.S., Chitty L. A study of voussoir arch. National Building Studies London: HMSO n.d.
[3] S. Gönen, S. Soyöz, Seismic analysis of a masonry arch bridge using multiple methodologies, Eng. Struct. (2021) 226, https://doi.org/10.1016/j.engstruct.2020.111354.
[4] B. Conde, L.F. Ramos, D. v Oliveira, B. Riveiro, M. Solla, Structural assessment of masonry arch bridges by combination of non-destructive testing techniques and three-dimensional numerical modelling: application to Vilanova bridge, Eng. Struct. 148 (2017) 621–638, https://doi.org/10.1016/j.engstruct.2017.07.011.
[5] B. Pulatsu, E. Erdogmus, P.B. Lourenço, Simulation of masonry arch bridges using 3D discrete element modeling, in: RILEM Bookseries, vol. 18, Springer,, Netherlands, 2019, pp. 871–880, https://doi.org/10.1007/978-3-319-99441-3_94.
[6] F. Cannizzaro, B. Pantò, S. Caddemi, I. Caliò, A discrete macro-element method (DMEM) for the nonlinear structural assessment of masonry arches, Eng. Struct. 168 (2018) 243–256, https://doi.org/10.1016/j.engstruct.2018.04.006.
[7] G. de Felice, Assessment of the load-carrying capacity of multi-span masonry arch bridges using fibre beam elements, Eng. Struct. 31 (2009) 1634–1647, https://doi.org/10.1016/j.engstruct.2009.02.022.
[8] B. Conde, L. Díaz-Vilariño, S. Lagüela, P. Arias, Structural analysis of Monforte de Lemos masonry arch bridge considering the influence of the geometry of the arches and fill material on the collapse load estimation, Constr. Build. Mater. 120 (2016) 630–642, https://doi.org/10.1016/j.conbuildmat.2016.05.107.
[9] V.N. Moreira, J. Fernandes, J.C. Matos, D.V. Oliveira, Reliability-based assessment of existing masonry arch railway bridges, Constr. Build. Mater. 115 (2016) 544–554, https://doi.org/10.1016/j.conbuildmat.2016.04.030.
[10] F. Accornero, G. Lacidogna, A. Carpinteri, Evolutionary fracture analysis of masonry arches: effects of shallowness ratio and size scale, Comptes Rendus - Mec. 344 (2016) 623–630, https://doi.org/10.1016/j.crme.2016.05.002.
[11] F. Accornero, G. Lacidogna, A. Carpinteri, Medieval arch bridges in the Lanzo Valleys, Italy: case studies on incremental structural analysis and fracturing benefit, J. Bridge Eng. (2018) 23, https://doi.org/10.1061/(asce)be.1943-5592.0001252.
[12] S. Gonen, B. Pulatsu, E. Erdogmus, P.B. Lourenço, S. Soyoz, Effects of spatial variability and correlation in stochastic discontinuum analysis of unreinforced masonry walls, Constr. Build. Mater. (2022) 337, https://doi.org/10.1016/j.conbuildmat.2022.127511.
[13] S. Gonen, B. Pulatsu, P.B. Lourenço, J. v Lemos, K. Tuncay, E. Erduran, Analysis and prediction of masonry wallette strength under combined compression-bending via stochastic computational modeling, Eng. Struct. (2023) 278, https://doi.org/10.1016/j.engstruct.2022.115492.
[14] J.C. Matos, V.N. Moreira, I.B. Valente, P.J.S. Cruz, L.C. Neves, N. Galvão, Probabilistic-based assessment of existing steel-concrete composite bridges – application to Sousa River Bridge, Eng. Struct. 181 (2019) 95–110, https://doi.org/10.1016/j.engstruct.2018.12.006.
[15] V.N. Moreira, J.C. Matos, D. v Oliveira, Probabilistic-based assessment of a masonry arch bridge considering inferential procedures, Eng. Struct. 134 (2017) 61–73, https://doi.org/10.1016/j.engstruct.2016.11.067.
[16] B. Conde, J.C. Matos, D. v Oliveira, B. Riveiro, Probabilistic-based structural assessment of a historic stone arch bridge, Struct. Infrastruct. Eng. 17 (2021) 379–391, https://doi.org/10.1080/15732479.2020.1752261.
[17] Z. Orbán, M. Gutermann, Assessment of masonry arch railway bridges using non-destructive in-situ testing methods, Eng. Struct. 31 (2009) 2287–2298, https://doi.org/10.1016/j.engstruct.2009.04.008.

[18] P. Borlenghi, A. Saisi, C. Gentile, ND testing and establishing models of a multi-span masonry arch bridge, J. Civ. Struct. Health Monit. (2023), https://doi.org/10.1007/s13349-022-00666-1.
[19] H. Park, H. Lee, H. Adeli, I. Lee, A new approach for health monitoring of structures: terrestrial laser scanning, Comput. Aided Civ. Infrastruct. Eng. 22 (1) (2007) 19–30, https://doi.org/10.1111/j.1467-8667.2006.00466.x.
[20] I. Lubowiecka, J. Armesto, P. Arias, H. Lorenzo, Historic bridge modelling using laser scanning, ground penetrating radar and finite element methods in the context of structural dynamics, Eng. Struct. 31 (2009) 2667–2676, https://doi.org/10.1016/j.engstruct.2009.06.018.
[21] D. Kang, H. Lee, H. Park, I. Lee, Computing method for estimating strain and stress of steel beams using terrestrial laser scanning and FEM, Key Eng. Mater. (2007) 347, https://doi.org/10.4028/www.scientific.net/KEM.347.517.
[22] N. Diamanti, A. Giannopoulos, M.C. Forde, Numerical modelling and experimental verification of GPR to investigate ring separation in brick masonry arch bridges, NDT E Int. 41 (2008) 354–363, https://doi.org/10.1016/j.ndteint.2008.01.006.
[23] L. Binda, G. Lenzi, A. Saisi, NDE of masonry structures: use of radar tests for the characterisation of stone masonries, NDTE Int. 31 (1998) 411–419.
[24] C. Colla, P.C. Dast, D. Mccann, Ford& MC. Sonic, electromagnetic and impulse radar investigation of stone masonry bridges, NDTE Int. 30 (1997) 249–254.
[25] Alvarado Blanco S., Durán Fuentes M., Nárdiz Ortiz C. Pontes históricas de Galicia. Colexio Oficial de Enxeñeiros de Camiños, Canais e Portos. Xunta de Galicia; 1991.
[26] I. Lubowiecka, P. Arias, B. Riveiro, M. Solla, Multidisciplinary approach to the assessment of historic structures based on the case of a masonry bridge in Galicia (Spain), Comput. Struct. 89 (2011) 1615–1627, https://doi.org/10.1016/j.compstruc.2011.04.016.
[27] B. Riveiro, P. Morer, P. Arias, I. de Arteaga, Terrestrial laser scanning and limit analysis of masonry arch bridges, Constr. Build. Mater. 25 (2011) 1726–1735, https://doi.org/10.1016/j.conbuildmat.2010.11.094.
[28] M. Solla, H. Lorenzo, A. Novo, J.C. Caamaño, Structural analysis of the Roman Bibei bridge (Spain) based on GPR data and numerical modelling, Autom. Constr. vol. 22 (2012) 334–339, https://doi.org/10.1016/j.autcon.2011.09.010.
[29] M. Solla, J.C. Caamaño, B. Riveiro, P. Arias, A novel methodology for the structural assessment of stone arches based on geometric data by integration of photogrammetry and ground-penetrating radar, Eng. Struct. 35 (2012) 296–306, https://doi.org/10.1016/j.engstruct.2011.11.004.
[30] Joint Committee on Structural Safety. Probabilistic Model Code. Part 1: Basis of design. 2000.
[31] Joint Committee on Structural Safety. Probabilistic Model Code. Part 2: Load Models. 2001.
[32] Ministero delle Infrastrutture e dei Transporti. Norme tecniche per le contruzioni. vol. 20. 2018.
[33] Joint Committee on Structural Safety. Probabilistic Model Code. Part 3: Resistance models. 2000.
[34] A. Cavicchi, L. Gambarotta, Two-dimensional finite element upper bound limit analysis of masonry bridges, Comput. Struct. 84 (2006) 2316–2328, https://doi.org/10.1016/j.compstruc.2006.08.048.
[35] D. v Oliveira, P.B. Lourenço, C. Lemos, Geometric issues and ultimate load capacity of masonry arch bridges from the northwest Iberian Peninsula, Eng. Struct. 32 (2010) 3955–3965, https://doi.org/10.1016/j.engstruct.2010.09.006.
[36] J. Heyman, The Stone Skeleton, vol. 2, Pergamon Press Ltd, 1966.
[37] Pippard A., Baker J. 1962:578.The voussoir arch. The Analysis of Engineering Structures.
[38] Gilbert M. Limit analysis applied to masonry arch bridges: state-of-the-art and recent developments. ARCH'07 - 5th International Conference on Arch Bridges Funchal, Madeira 2007:13–28.
[39] G. Milani, P.B. Lourenço, 3D non-linear behavior of masonry arch bridges, Comput. Struct. 110–111 (2012) 133–150, https://doi.org/10.1016/j.compstruc.2012.07.008.
[40] B. Pulatsu, E. Erdogmus, P.B. Lourenço, Comparison of in-plane and out-of-plane failure modes of masonry arch bridges using discontinuum analysis, Eng. Struct. 178 (2019) 24–36, https://doi.org/10.1016/j.engstruct.2018.10.016.
[41] P. Zampieri, M.A. Zanini, F. Faleschini, L. Hofer, C. Pellegrino, Failure analysis of masonry arch bridges subject to local pier scour, Eng. Fail Anal. 79 (2017) 371–384, https://doi.org/10.1016/j.engfailanal.2017.05.028.
[42] European Committee for Standardization. Eurocode 1: Actions on structures. Part 2: Traffic loads on bridges (EN 1991–2). Brussels: 2019.
[43] A.S. Nowak, K.R. Collins. Reliability of Structures, 2nd ed., CRC Press, 2012.
[44] N. Galvão, J.C. Matos, D. v Oliveira, R. Hajdin, Human error impact in structural safety of a reinforced concrete bridge, Struct. Infrastruct. Eng. 18 (2022) 836–850, https://doi.org/10.1080/15732479.2021.1876105.
[45] J.C. Matos, P.J.S. Cruz, I.B. Valente, L.C. Neves, V.N. Moreira, An innovative framework for probabilistic-based structural assessment with an application to existing reinforced concrete structures, Eng. Struct. 111 (2016) 552–564, https://doi.org/10.1016/j.engstruct.2015.12.040.
[46] European Committee for Standardization. Eurocode. Basis of structural design (EN 1990). Brussels: 2019.
[47] International Organization for Standardization. General principles on reliability for structures (ISO 2394:2015). 2015.
[48] International Organization for Standardization. Bases for design of structures - Assessment of existing structures (ISO 13822). 2012.
[49] J. Sacks, W.J. Welch, T.J. Mitchell, H.P. Wynn, Design and analysis of computer experiments, Stat. Sci. 4 (4) (1989) 409–423, https://doi.org/10.1214/ss/1177012413.
[50] Lataniotis C., Wicaksono D., Marelli S., Sudret B. Uqlab User Manual Kriging (Gaussian Process Modeling). n.d.
[51] A. Saltelli, M. Ratto, T. Andres, F. Campolongo, J. Cariboni, D. Gatelli, et al., Global sensitivity analysis. The Primer, Chichester: John Wiley & Sons, Ltd, 2008.
[52] Marelli S., Lamas C., Konakli K., Mylonas C., Wiederkehr P., Sudret B. Uqlab User Manual Sensitivity Analysis. n.d.
[53] A. Gelman, J.B. Carlin, H.S. Stern, D.B. Dunson, A. Vehtari, D.B. Rubin. Bayesian Data Analysis, 3rd ed., CRC Press, 2014.